Absolute determination of the layer-perpendicular band structure of VSe_2 and TiS_2 by combined very-low-energy electron diffraction and photoemission

1998 J. Phys.: Condens. Matter 10 5749

(http://iopscience.iop.org/0953-8984/10/26/004)

J. Phys.: Condens. Matter **10** (1998) 5749–5766. Printed in the UK PII: S0953-8984(98)91860-4

Absolute determination of the layer-perpendicular band structure of VSe_2 and TiS_2 by combined very-low-energy electron diffraction and photoemission

V N Strocov†§, H I Starnberg†, P O Nilsson†, H E Brauer† and L J Holleboom‡

† Department of Physics, Chalmers University of Technology and Göteborg University, SE-412 96 Göteborg, Sweden

‡ Department of Theoretical Physics, University of Lund, SE-223 62 Lund, Sweden

Received 16 February 1998

Abstract. The layer-perpendicular dispersions $E(k_\perp)$ of the typical layered TMDCs VSe_2 and TiS_2 were studied by combining determination of the upper unoccupied bands by very-low-energy electron diffraction (VLEED) with mapping of the lower occupied bands by photoemission (PE). We found that the upper bands of these materials are very complicated, and are compatible neither with the free-electron, nor with the ground-state approximation. Knowledge of the upper bands allowed us to carry out a PE experiment optimized for the $k_\perp$-resolved mapping of the lower bands. The PE data were consistently rationalized, using a map of the PE intensity as a function of the binding energy E_i and the photon energy $h\nu$. We found that the PE intensity is well described by direct, $k_\perp$-conserving, transitions, with minor shifts of PE peaks being basically a consequence of their broadening due to finite electron and hole lifetime. Finally the lower bands were mapped explicitly, using the PE peaks with minimal shifts and the experimental upper bands. The obtained $E(k_\perp)$ is very consistent, and shows overall agreement with full-potential LAPW calculations.

1. Introduction

VSe_2 and TiS_2 are typical layered transition metal dichalcogenides (TMDCs). These materials crystallize as a stack of weakly bound layers, each layer consisting of a sheet of metal atoms between two sheets of chalcogen atoms. As the inter-layer bonding is much weaker than the intra-layer bonding, TMDCs have highly anisotropic, quasi-two-dimensional physical properties. This atomic structure gives rise to many interesting and practically important phenomena (Friend and Yoffe 1987).

The electronic band structures $E(\boldsymbol{k})$ of TMDCs have been extensively studied by photoemission (PE) (Anderson *et al* 1985, Pehlke *et al* 1990a, b, Starnberg *et al* 1993, 1994, Claessen *et al* 1996) and inverse photoemission (Straub *et al* 1985, Law *et al* 1991, Langlais *et al* 1995). It was found that, although the dispersion $E(\boldsymbol{k}_\parallel)$ parallel to the layers is in general stronger than the dispersion $E(k_\perp)$ perpendicular to the layers, $E(k_\perp)$ remains significant. Explicit PE mapping of $E(k_\perp)$ of the occupied lower bands, conventionally using for the unoccupied *upper bands* (UBs) the free-electron approximation, failed however to produce any consistent results. Moreover, it was

§ Also with the Institute for High-Performance Computations and Data Bases, PO Box 71, 194291 St Petersburg, Russia.

0953-8984/98/265749+18$19.50

shown that final states could comprise multiple UBs (Pehlke and Schattke 1987a). These facts indicated a complicated structure of UBs of TMDCs, incompatible with the free-electron approximation. Accurate bandmapping required us therefore to determine the UBs independently.

The UBs are directly accessed by very-low-energy electron diffraction (VLEED), whose energy range is typically 0–35 eV above the vacuum level E_{vac}. VLEED is connected to PE is because the PE final states, neglecting the electron–hole interaction, are exactly the time-reversed LEED states (Feibelman and Eastman 1974, Pendry 1976, Jepsen *et al* 1982). The energy range of VLEED fits the typical final state energies in PE bandmapping.

Basically, VLEED reveals irregularities in $E(k_\perp)$. This is clear from matching of the wavefunction in vacuum Φ_v (the superposition of the incident and all diffracted plane waves) to the wavefunction excited in the crystal Φ_c (the superposition $\Phi_c = \sum_n T_n \phi_n$ of the excited-state Bloch waves ϕ_n, available under conservation of incident energy E and surface-parallel momentum $\boldsymbol{K}_\parallel$) (Capart 1969, Pendry 1974, Jaklevic and Davis 1982). The changes in the elastic electron reflection $R(E)$, or transmission $T(E) = 1 - R(E)$, are then connected to changes in Bloch waves near irregularities of the excited-state $E(k_\perp)$ along the direction(s) $\boldsymbol{k}_\parallel = \boldsymbol{K}_\parallel + \boldsymbol{g}$ in the Brillouin zone (BZ), $\boldsymbol{g}$ being surface reciprocal vectors. Quantitatively (Strocov 1991, 1995, Strocov *et al* 1996a), the changes in the $T(E)$ are identified as the $\mathrm{d}T/\mathrm{d}E$ extrema, and the irregularities in the excited-state $E(k_\perp)$ as the *irregularity points* (IPs), characterized by the extrema in $\mathrm{d}^2 \operatorname{Re} k_\perp / \mathrm{d}E^2$. The crucial point is that the $\mathrm{d}T/\mathrm{d}E$ extrema are all due to the IPs only in the *coupling bands*. These bands are characterized by large *partial transmissions* (PTs), which are $|T_n|^2$ implying the normalization $\int \phi_n^* \phi_n \, \mathrm{d}\boldsymbol{r} = 1$ in the crystal half-space. (PTs are approximately proportional to the *partial absorbed currents* into the crystal $I_n \propto V_i |T_n|^2$.)

In practical VLEED band determination (Strocov 1991, 1995, Strocov *et al* 1996a, 1997a, b), one (1) establishes an explicit connection of the $T(E)$ to the $E(k_\perp)$, carrying out a matching-type approximate *reference calculation*; (2) determines the experimental position of the coupling-band IPs by correcting their reference energies by the energy difference between the experimental and reference energies of the $\mathrm{d}T/\mathrm{d}E$ extrema; (3) determines continuous bands, in $E(\boldsymbol{k}_\parallel)$ by point-by-point mapping the experimental IPs as a function of $\boldsymbol{K}_\parallel$, and in $E(k_\perp)$ by a *reference-band interpolation*, or by *band fitting* between the experimental IPs. The procedure may be simplified by neglecting the absorption V_i (*no-absorption* (NA) *approximation*) (Strocov *et al* 1996a, Strocov 1998). In this case one analyses the excited-state IPs as ordinary *critical points* (CPs), and PTs, which in principle become infinite, as the partial absorbed currents.

VLEED band determination provides the UBs, which (1) are corrected from vague approximations or computational inaccuracies, and (2) absorb true, experimental, self-energy corrections. Their use in PE bandmapping (Strocov *et al* 1997b) allows one to achieve *absolute* determination of $E(\boldsymbol{k})$, which is free from limiting approximations, and covers both upper and lower bands.

We report on the application of combined VLEED and PE to resolve $E(k_\perp)$ of layered VSe_2 and TiS_2, concentrating on the ΓA direction in the BZ. Our procedure includes (1) determination of the UBs by VLEED, and using these data for (2) optimization of the PE bandmapping experiment, and (3) explicit PE mapping of the lower bands. This paper extends our recent work on VSe_2 (Strocov *et al* 1997b). Comparing to our previous studies (Strocov *et al* 1996b), we have greatly improved the experimental accuracy and the data analysis procedure.

2. Unoccupied upper bands

2.1. VLEED experiment

The VLEED experiment was carried out with a standard four-grid LEED unit (Strocov and Starnberg 1995). To operate the electron gun down to the lowest kinetic energies we used the retarding field mode: the grids and the last electron gun electrode were biased by +300 V relative to the cathode, with the sample at ground potential. Using explicit ray tracing calculations (Strocov 1996), we analysed the operation of our setup, and found very strong sensitivity of the electron trajectories to any asymmetries in the electron optics. In particular, we used a standard manipulator; being asymmetrical in the vertical plane, the manipulator at the ground potential caused a field asymmetry, which resulted in a vertical deviation of the electron beam with energy-dependent uncompensated $\boldsymbol{K}_\parallel$ up to 0.15 Å^{-1}. Very neatly, this effect was removed by attaching a metal symmetrizing shield below the manipulator. Other parts of the electron optics were also carefully aligned. These measures were crucial for a precise VLEED experiment. The beam diameter was finally smaller than 1.5 mm down to zero kinetic energy, and the $\boldsymbol{K}_\parallel$ divergence produced energy spread less than 0.3 eV HWHM. We measured the elastic transmission spectra $T(E)$ by the target-current-spectroscopy (TCS) technique: the current absorbed by the sample $I(E)$ is recorded; as the inelastic contribution to $I(E)$ is a smoothly varying function, the structure of $I(E)$ is due to the elastic component, $T(E) \propto I(E)$.

The samples were cleaved *in situ*, and produced sharp LEED patterns. The normal incidence angle was adjusted to within $\pm 0.5^\circ$ as corresponding to the extremal positions of the spectral features under variation of the incidence angle in two perpendicular azimuths. The workfunction $e\phi$ was 5.6 ± 0.1 eV for VSe_2, and 5.8 ± 0.1 eV for TiS_2. All spectral features showed apparent angular dispersion, which confirmed their elastic origin. For TiS_2, comparing to the previous study (Strocov *et al* 1995) we found larger $e\phi$, and did not detect surface resonance structures, which may be due to less perfect surface quality. Except this, the spectral features were largely identical to the previous data; the present spectra are, however, more accurate because of the optimization of the electron optics.

2.2. Band determination procedure

2.2.1. Reference calculations. A reference calculation was made in the NA approximation, as reliable excited-state calculations on VSe_2 or TiS_2 are presently lacking. We calculated $E(\boldsymbol{k})$ within the LDA–DFT approximation using the self-consistent full-potential linearized-augmented-plane-wave (LAPW) method. (A VLEED band determination largely relies on that the reference calculations give not necessarily accurate energy position, but relevant configuration of $E(\boldsymbol{k})$. From our experience, for TMDCs the best in this respect are self-consistent and full-potential LAPW calculations.) On top of $E(k_\perp)$ calculations, we found the corresponding PTs $|T_n|^2$ (strictly speaking, partial absorbed currents I_n) and the total $T(E)$, using the conducting-Fourier-component–group-velocity (CFC–v_g) approximation (Strocov 1998) with the Fourier expansion $\sum_{\boldsymbol{G}} C_n^{\boldsymbol{G}} \, \mathrm{e}^{\mathrm{i}(\boldsymbol{k}+\boldsymbol{G})\cdot\boldsymbol{r}}$ of the LAPW Bloch waves in the interstitial region. To evaluate $T(E)$ within an accuracy of ± 0.05 eV, we sampled $k_\perp$ in steps of $0.01|\Gamma A|$. (The advantage of the CFC–v_g approximation, compared to explicit matching calculations, is that the PTs and $T(E)$ are found as a by-product of bulk band calculations at almost no additional runtime. Although this approximation may somewhat compromise the amplitudes of $T(E)$ features, their energies are accurate. This property makes it adequate for VLEED band determination.)

The effect of absorption V_i is simulated in total $T(E)$ by (1) damping the $T(E)$ variations as $T(E)(1 - V_i(E)/V_i^{out})$, where $V_i(E) = V_i^{out}$ corresponds to complete damping of the elastic structures, $V_i^{out} \approx 3$ eV, and (2) Lorentzian smoothing with the halfwidth $V_i(E)$. We modelled the absorption V_i by a linear function of energy with a Fermi–Dirac-like step $\propto [1 + \exp(-(E - \overline{h}\omega_p)/3.0)]^{-1}$, added at the plasmon threshold $\overline{h}\omega_p \approx 21.5$ eV (Pehlke *et al* 1990b). The parameters of this dependence were first estimated roughly by comparison of the reference $\mathrm{d}T/\mathrm{d}E$ curves with the experimental, and then refined from the $\mathrm{d}T/\mathrm{d}E$ curves calculated on top of the experimental $E(\boldsymbol{k})$, as discussed below.

2.2.2. Estimation of the absorption V_i. The absorption V_i may be estimated from the broadening of VLEED spectral structures. This requires however a sort of fitting of the experimental spectra by reference calculations, as apart from the main contribution from V_i the broadening is influenced by variations of elastic $T(E)$ within the spectral structures.

We characterized the broadening at the left and right side of every $\mathrm{d}T/\mathrm{d}E$ extremum. Numerically, we expressed the broadening as the differences ΔE_B between the energy of the $\mathrm{d}T/\mathrm{d}E$ extremum ($\mathrm{d}T/\mathrm{d}E = 0$), and the energies of the left-side and right-side inflexion points ($\mathrm{d}^2T/\mathrm{d}E^2 = 0$). This quantification is insensitive to the amplitudes and energies of the $\mathrm{d}T/\mathrm{d}E$ features. Then we fitted each ΔE_B by the reference calculations, varying V_i. Below $E = 4$ eV, where the correspondence between the experimental and reference $\mathrm{d}T/\mathrm{d}E$ was good and spectral structures sharp, the fitting gave us V_i rather accurately. For VSe_2 $V_i = 0.32 \pm 0.05$ eV at $E = 6.8$ eV, and increases to 0.55 ± 0.1 eV at $E = 8.7$ eV; for TiS_2 $V_i = 0.40 \pm 0.05$ eV at $E = 6.2$ eV, and 0.5 ± 0.05 eV at $E = 8.6$ eV. Above $E = 10$ eV, V_i increases further, and the influence of the elastic component in the broadening makes the V_i determination less accurate. We determined V_i there approximately, from the overall shape of the spectral structures. Finally, for VSe_2 we obtained, energies in eV, $V_i(E) = 0.3 + 0.04(E - e\phi) + 1.0[1 + \exp(-(E - \overline{h}\omega_p)/3.0)]^{-1}$, and for TiS_2 $0.35 + 0.04(E - e\phi) + 1.2[1 + \exp(-(E - \overline{h}\omega_p)/2.5)]^{-1}$.

2.2.3. Band determination in the NA approximation. The UBs were determined in the NA approximation, and after that the excited-state band smoothing was simulated.

For VSe_2, the band determination along A is illustrated in figure 1 (left). First, we found how CPs of the reference $E(k_\perp)$ are connected with the extrema of the corresponding normal-incidence reference $\mathrm{d}T/\mathrm{d}E$: In the reference $E(k_\perp)$ in figure 1(a), we identified the coupling bands as those having substantial $|T_n|^2$. All their CPs, which are associated with sharp variations of the wavefunction in the solid, produce steplike changes in the reference no-absorption $T(E)$ calculated with $V_i = 0$, figure 1(b). With realistic V_i, these changes are smoothed and are more clear in $\mathrm{d}T/\mathrm{d}E$, figure 1(c, upper curve). Below $E = 14$ eV, V_i is less than 0.6 eV. As this is less than or about the energy differences between the adjacent CPs, every coupling band CP is one-to-one connected to an extremum in $\mathrm{d}T/\mathrm{d}E$. At higher energies V_i increases, and the extrema in $\mathrm{d}T/\mathrm{d}E$ from adjacent CPs overlap. For example, the $\mathrm{d}T/\mathrm{d}E$ maximum near 15 eV is due to two CPs, at 14.5 eV and 15.5 eV. The position of a resulting $\mathrm{d}T/\mathrm{d}E$ extremum depends then on the positions of several adjacent CPs, and also on the amplitudes of the associated changes in the no-absorption $T(E)$; a direct one-to-one correspondence may not be established. Above the plasmon threshold $\overline{h}\omega_p \approx 21.5$ eV V_i increases to 1.5–2.5 eV, which causes the $\mathrm{d}T/\mathrm{d}E$ structure to smooth out.

Second, we compared the reference $\mathrm{d}T/\mathrm{d}E$ with the experimental one, figure 1(c, lower curve): on average, the experimental extrema (and the associated CPs) occur at 0.7 eV higher energy. This figure gives an estimate for the self-energy correction $\mathrm{Re}\,\Delta\Sigma$.

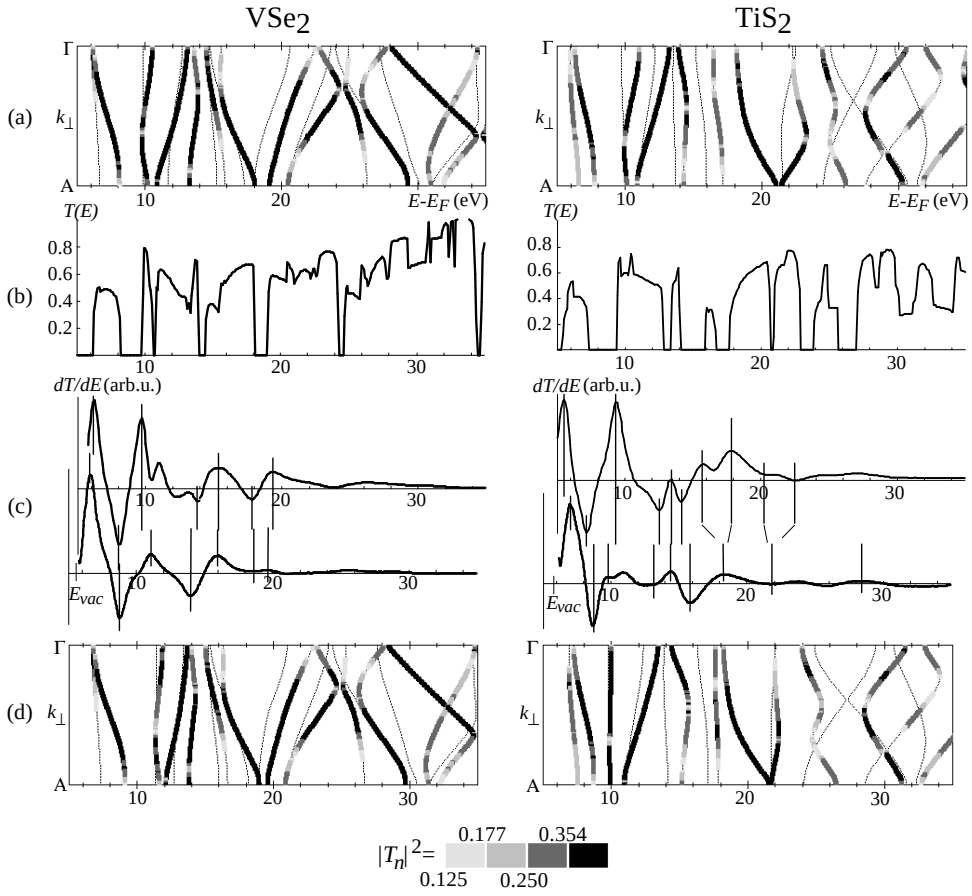

Figure 1. VLEED band determination in the NA approximation: (a) calculated reference $E(k_\perp)$ along ΓA, with the PTs $|T_n|^2$ shown in greyscale; (b) the associated normal-incidence reference $T(E)$, calculated with $V_i = 0$, and (c, upper curve) $\mathrm{d}T/\mathrm{d}E$, calculated with optimized V_i. (c, lower curve) The experimental $\mathrm{d}T/\mathrm{d}E$, with the correspondence of reference and experimental $\mathrm{d}T/\mathrm{d}E$ extrema shown; (d) experimental no-absorption $E(k_\perp)$, obtained by interpolation between the CPs.

The poor agreement between 9 eV and 14 eV seems to be due to instability of band calculations in this region. Experimentally, the simple minimum–maximum structure of the experimental $\mathrm{d}T/\mathrm{d}E$ in this region suggest, that the variations in $T(E)$ are negligible, and that the band gap widths are considerably less than V_i. We therefore have connected the experimental minimum–maximum with the edges of the band manifold in this region, as shown in the figure. (Two shoulders in the experimental $\mathrm{d}T/\mathrm{d}E$ at 4.5 eV and 7 eV do not correspond to the calculated maxima at 4.2 eV and 7.6 eV; such shoulders appear whenever a Lorentzian-like minimum and maximum slightly overlap.) Everywhere else, the one-to-one correspondence between the experimental and reference $\mathrm{d}T/\mathrm{d}E$ extrema is clear. Their energy shifts were used to map out the experimental CPs: we energy corrected the reference CPs, keeping them at the same $k_\perp$.

Third, we recovered the whole experimental no-absorption bands between the experimental CPs, figure 1(d). We applied band interpolation: the reference bands

were energy shifted, with the shift piecewisely linearly varying between the fixed energy shifts at the experimental CPs. The correction above the highest-energy CP was taken constant and equal to the correction in this CP. The PTs were left equal to the reference values.

It should be noted that our procedure might less accurately place the non-coupling bands, which are characterized by $|T_n|^2 \approx 0$ and therefore not seen in VLEED. These bands give however negligible contribution in PE also. Non-coupling bands may usually be mapped in a point-by-point manner from measurements on another surfaces (Strocov 1995, Strocov *et al* 1996a), but those do not exist for layered materials.

For TiS_2, the same procedure is shown in figure 1 (right). Compared to VSe_2, the reference calculations show larger band gap widths; despite larger V_i, this results in notable structure of the dT/dE above the plasmon threshold. The experimental dT/dE extrema are on average at 1.0 eV higher energy relative to the corresponding reference ones. Compared to VSe_2, the agreement between the reference and experimental dT/dE is notably worse, which is a defect of the LAPW calculations. In particular, (1) a faint maximum–minimum structure in the experimental dT/dE near 10 eV shows that the associated flat reference band is well separated from the higher-placed band, and its PT is smaller than calculated. Then the experimental maximum at 10.9 eV corresponds to the onset of the reference band at 10.3 eV; (2) the reference maxima at 15.7 eV and 17.8 eV experimentally merge. The associated band lower edges are therefore separated from the higher-energy band by less than $V_i/2$; (3) the reference minima at 20.0 eV and 22.6 eV experimentally merge. The associated band higher edges are therefore also separated by less than $V_i/2$. With these considerations, we set the dT/dE extrema correspondence as shown in the figure, and mapped the coupling band CPs. (The higher-energy CPs may be less accurate, as larger V_i makes the energies of the dT/dE extrema more sensitive to the CFC–V_g amplitude inaccuracy.) The experimental bands appeared significantly different from the reference bands. This suggests that the band determination may be less accurate, comparing to VSe_2.

2.2.4. Simulation of excited-state band smoothing. The UBs are essentially the excited-state bands of the complex energy $E + iV_i$, depending on the complex wavevector $\mathrm{Re}\boldsymbol{k} + \mathrm{Im}\,\boldsymbol{k}$ (Pendry 1974, Goldmann *et al* 1991, Strocov *et al* 1996a). For brevity, in the following we refer to $E(\mathrm{Re}\,\boldsymbol{k})$ as the excited-state bands too. Commonly in LEED and PE, the excited-state effects are described empirically, by modelling the excited-state potential (1) by the ground-state potential with an empirical E- and $\boldsymbol{k}$-dependent self-energy correction, for the Hermitian part, and (2) by the absorption V_i, for the non-Hermitian part. The excited-state bands $E(\mathrm{Re}\,\boldsymbol{k})$ differ from the ground-state bands $\varepsilon(\boldsymbol{k})$ in two aspects: (1) They are systematically energy shifted from $\varepsilon(\boldsymbol{k})$, and (2) smoothed near the band gaps of $\varepsilon(\boldsymbol{k})$. In the present band determination, the systematic shifts are already absorbed in the experimental no-absorption bands in figure 1(d). The band smoothing was simulated as follows.

In the no-absorption experimental $E(k_\perp)$, we identified two principal branches in the coupling bands. We tentatively appended each branch by real lines across the band gaps, and by the real line $\mathrm{Re}\,\boldsymbol{k} = \text{constant}$ going from $E = -\infty$ to its bottom, figure 2(a). Then each branch was energy sampled in steps of 0.1 eV, represented as $k_\perp(E)$ in the extended zone scheme, Lorentzian smoothed with the halfwidth $V_i(E)$ and folded back to the first BZ. The results are shown in figure 2(b). These are the principal experimental UBs in VLEED and PE, which are required as the UBs in PE bandmapping. Not included in the simulation were the bands with small PT; they however give slight contribution in both VLEED and PE. We stress that our simulation of the band smoothing was tentative.

The band determination procedure may be refined, particularly at this point, if based on excited-state calculations, at least empirical.

A straightforward technique to simulate the excited-state effects on top of ground-state bandstructure is the exact $\boldsymbol{k}\cdot\boldsymbol{p}$ method (Krasovskii and Schattke 1997) including V_i.

Not included in the simulation were the bands with small PT; they however give slight contribution in both VLEED and PE.

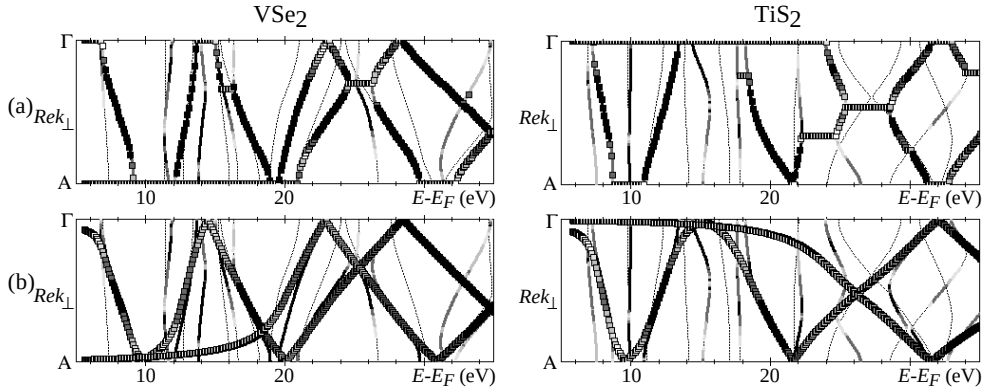

Figure 2. Simulation of the excited-state smoothing of the upper bands: (a) The principal coupling band branches in no-absorption experimental bands from figure 1(d), appended by tentative real lines (bold dashed lines). These branches are shown sampled in the energy steps 0.1 eV, with the PTs $|T_n|^2$ in the greyscale of figure 1. (b) The excited-state smoothed principal coupling bands, the upper bands in PE bandmapping.

2.3. Properties of the experimental UBs

Despite the excited-state smoothing, the experimental UBs of VSe_2 and TiS_2 remain far from free-electron-like bands in that (1) they feature two branches of the bands, and (2) each branch may be approximated by a free-electron parabola $E = \hbar^2(\boldsymbol{k}+\boldsymbol{G})^2/2m + V_{000}$ only locally, i.e. the inner potential V_{000} strongly depends on E and $\boldsymbol{k}_\parallel$. We illustrate this by the results of local free-electron fitting for VSe_2. Along ΓA, fitting of the steeper branch in the energy range from 6 eV to 23 eV gave V_{000} varying from +10.2 eV to +13.3 eV. (Note placement of the free-electron parabola bottoms well above E_{vac}. It is about 15 eV higher than usual placements near the valence band bottom.) Along the BZ direction $\boldsymbol{k}_\parallel = 0.5$ ΓK, where we determined the UBs from the corresponding off-symmetry VLEED data (Strocov *et al* 1996b) there was a single branch in the same energy range; the fitting gave V_{000} very different, and also varying from +5.5 eV to +8.1 eV. For TiS_2 the deviations from free-electron bands are even larger.

The UBs, experimentally determined as described from VLEED data, enable very accurate PE bandmapping of the lower bands, as they (1) are corrected from band calculation inaccuracies, and (2) include the true, experimental, self-energy corrections.

2.4. Optimization of the PE experiment for $k_\perp$-resolved bandmapping

The experimental UBs were now used to optimize the PE experiment. From the VLEED-derived UBs, and the LAPW-calculated lower bands, we constructed the structure plots in

figure 3. (The analyses do not depend critically on a particular shape of the lower bands; one may use any monotonic curves, connecting the band edges in Γ and A.)

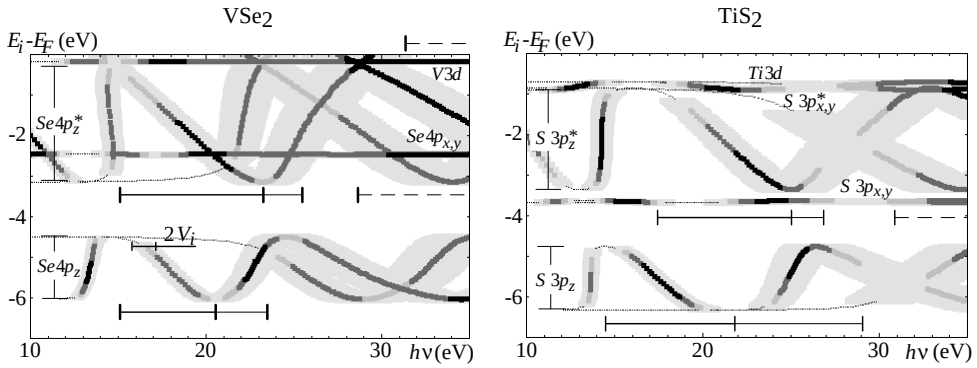

Figure 3. PE structure plot from the experimental upper bands, and the LAPW calculated lower bands. PTs $|T_n|^2$ are shown in the greyscale of figure 1. Where $|T_n|^2$ is substantial, the FWHM peak broadening is shown by shading. The accurate bandmapping $h\nu$ ranges are indicated as bold lines, less accurate as thin lines and less accurate where the upper bands are rough as dashed lines.

To explain this construction, we recall some facts from the one-step theory of PE. If the absorption V_i in the final state is weak, the peak of the PE intensity from the n'th initial-state Bloch wave to the nth final-state Bloch wave appears in $\boldsymbol{k}$-space as a Lorentzian $|\Delta_{n'n}|^2$, whose amplitude is proportional to the one-dimensional DOS $|\mathrm{d}k_\perp^{n'}/\mathrm{d}E_i|$, matrix element $|M_{n'n}|^2$ and PT $|T_n|^2$:

$$I \propto |\mathrm{d}k_\perp^{n'}/\mathrm{d}E_i||M_{n'n}||T_{n'n}||\Delta_{n'n}|^2. \tag{1}$$

$|\Delta_{n'n}|^2$ is centred in the $k_\perp$-conserving position, and has the $k_\perp$-broadening $2\Delta k_\perp$. $\Delta k_\perp$ is determined as $\Delta k_\perp = \mathrm{Im}\,k_\perp^n + \mathrm{Im}\,k_\perp^{n'}$, where $\mathrm{Im}\,k_\perp = V_i/v_{g\perp}$, with V_i and $v_{g\perp}$ being the final-state and initial-state absorption and perpendicular group velocity correspondingly; the absorption is connected to the lifetime as $V_i = \hbar/\tau$ (Feibelman and Eastman 1974, Jepsen *et al* 1982, Smith *et al* 1993, Strocov *et al* 1997a). (A more rigorous approach is that a PE peak appears due to the $k_\perp$-broadening only in the final state $\Delta 2k_\perp = 2\,\mathrm{Im}\,k_\perp$ combined with the hole-lifetime energy broadening of the initial state (Matzdorf 1996). In principle, the two approaches are equivalent only if the dispersion $E(k_\perp)$ is linear. We adopt the first for simplicity.)

The structure plots in figure 3 show, for every photon energy $h\nu$, the lower band energies $E_i - E_F$, for which a direct transition to an UB is possible. The corresponding PE peaks are Lorentzians (1). Of their amplitude factors, the PTs are shown in greyscale. The Lorentzians have a broadening (Smith *et al* 1993), which is most conveniently determined in the constant-initial-state mode $E_i - E_F =$ constant: they are $2V_i$ FWHM wide, neglecting the hole lifetime. This is shown by shading, which is $2V_i$ horizontally. The vertical cuts $h\nu =$ constant of the plots correspond to the energy-distribution-curve (EDC) spectra, and the horizontal cuts $E_i - E_F =$ constant to the constant-initial-state (CIS) spectra.

For reliable $k_\perp$-resolved bandmapping (Strocov *et al* 1996b), the PE peaks should be (1) clearly resolved from adjacent peaks, and (2) sufficiently narrow compared to the bandwidth, that variations of the intensity factors $|\mathrm{d}k_\perp^{n'}/\mathrm{d}E_i|$, $|M_{n'n}|^2$, or PT within the peak widths do not shift the peaks from the $k_\perp$-conserving positions (Feibelman and Eastman

1974, Pehlke and Schattke 1989, Pehlke *et al* 1990b, Strocov *et al* 1996b). Because of rather weak perpendicular dispersion $E(k_\perp)$, the latter condition is particularly restrictive for the layered crystals.

Analysing the structure plot according to these criteria in the EDC mode, we sorted out the *accurate* and *less-accurate bandmapping* regions, as indicated in figure 3. (A nearly vertical branch of the structure plot near $h\nu = 14$ eV may not be used for bandmapping in the EDC mode; however, in the CIS mode it may.) For VSe_2 and TiS_2 the regions somewhat differ. We stress two points: (1) To obtain sufficient $k_\perp$-sampling in the accurate bandmapping regions, because of flatness of the upper bands, $h\nu$ should be changed in steps finer than 0.5 eV; (2) the accurate bandmapping regions are all at lower $h\nu$, which correspond to the final-state energies $E - E_F$ below the plasmon threshold $\hbar\nu_p \approx 21.5$ eV. At larger $h\nu$ the peaks broaden, which potentially shifts the peaks from the $k_\perp$-conserving positions and makes bandmapping less accurate. At $h\nu$ above ≈30 eV the peaks from the two different UBs are resolved, and may also be used in bandmapping, although less accurate, with the two UBs; however, our VLEED band determination was potentially less accurate in this region, as we had here no experimental CPs.

It should be noted that the PE bandmapping experiments optimal for TMDCs differ significantly from common practice because of a complicated structure of their UBs.

3. Occupied lower bands

3.1. PE experiment and the data processing

The PE experiment according to the VLEED-derived recipe was done at the MAX-lab synchrotron radiation facility, Lund, Sweden. We measured EDCs $I(E_i)$ at normal emission. The normal emission was adjusted moving the analyser in two perpendicular azimuths as corresponding to extremal behaviour of the spectral features. We changed $h\nu$ in 0.25 eV steps below ≈25 eV, which covered the accurate bandmapping ranges, and in 0.5 eV steps above. Our experimental results agree with the previous study carried out in a narrower $h\nu$-range (Anderson *et al* 1985, Pehlke *et al* 1990a).

Numerical processing of the EDCs included: (1) denoising by Gaussian smoothing using the HWHM 0.075 eV; (2) subtracting a constant inelastic background, estimated from the spectral intensity above E_F; (3) intensity normalization. This was particularly important, as the experimental data were measured over three to five injections, with the light intensity varying. We found it inappropriate to normalize by the current in the storage ring, because the light intensity depends also on the alignment of the electron beam in the ring, which varies from injection to injection, and even somewhat fluctuates within one injection. Very neatly, normalization might be achieved by measuring any one CIS spectrum $I(E_i, h\nu)$, and scaling the EDCs according to their intensity at the same E_i; unfortunately, our experimental setup did not operate in the CIS mode. We therefore chose to normalize the spectra from the intensity integrated within the valleys between the spectral peaks (*in-valley normalization*). This normalization is less sensitive to the peak positions and intensities, which depend on $h\nu$. We identified the valleys as $\mathrm{d}^2I/\mathrm{d}E_i^2 > 0$ in the spectra denoised with HWHM ≈ 0.15 eV. (4) Smoothing of the $h\nu$-variations. Each EDC was multiplied by a factor α, which minimizes the mean-square difference $\langle\Delta^2\rangle$ of this EDC $I(E_i)$ from the two adjacent-$h\nu$ EDCs $I^-(E_i)$ and $I^+(E_i)$, $\langle\Delta^2\rangle \propto \sum_i[\alpha I(E_i) - [I^-(E_i) + I^+(E_i)]/2]^2$, where i numerates the data points. This factor may therefore be found from the condition $\mathrm{d}\langle\Delta^2\rangle/\mathrm{d}\alpha = 0$, which yields $\alpha = \frac{1}{2}(\sum_i[I_i(E_i)\chi I_i^-(E) + I_i^+(E)\eta])/\sum_i[I(E_i)]^2$. This procedure was applied iteratively three to five times.

The EDCs were then rendered to a two-dimensional greyscale map of the PE intensity $I(E_i, h\nu)$ in figure 4(a). The contrast was increased by subtracting a smooth background, obtained in every $(E_i, h\nu)$-point by local averaging of the intensity within few eV wide circular areas around this point. (This procedure suppresses the smoothly varying intensity from the inelastic SEE processes as well as the intensity from the non-$k_\perp$-conserving transitions, which sharply increases if within the band energy ranges.) The map in fact combines the EDC mode (vertical cuts $h\nu$ = constant) with the CIS mode (horizontal cuts E_i = constant), and the constant-final-state (CFS) mode (cuts along the lines $E_i + h\nu$ = constant) in one single representation. This intensity map enabled a very clear and effective identification of the PE peaks.

An interesting modification of this map, a 'flattened' intensity map, in figure 4(b) shows the EDC peaks $\mathrm{d}^2 I/\mathrm{d}E_i^2 < 0$ by white, and the valleys by black, independently of intensity. This modification clearly shows even very slight shoulder-like EDC peaks, like that for TiS_2 near $E_i = -0.1$ eV. A disadvantage of this representation is that it needs heavy smoothing, HWHM ≈ 0.15 eV. This results in considerable shifting of shoulder-like peaks, and hiding of the saddle-point-like peaks, which are extremal in CIS spectra E_i = constant but not in EDC spectra $h\nu$ = constant.

3.2. Data interpretation

3.2.1. Rationalization of the PE peaks. Some peaks are clearly irrelevant to the valence-band lower bands: (1) the peaks seen as sharply ascending straight lines (ascending dashes) are core level peaks, excited by higher-order-diffraction light; (2) the peaks seen as descending straight lines (descending dashes) are due to secondary electron emission (SEE). This is because they have a constant energy $E_i + h\nu$ = constant (descending dashes), exist even above E_F and cross the band gaps without intensity changes. (These peaks seem to enchance when crossing the energy regions of the valence bands; the SEE intensity however does not change here, but appears on top of non-$k_\perp$-conserving PE intensity from these bands.) SEE peaks appear from flat UBs, which have high one-dimensional DOS and sufficient PTs. Such bands may easily be seen in figure 1(d): for VSe_2 the two SEE peaks appear from two such bands near 8.0 eV and 10.5 eV, and for TiS_2 from the band near 10.0 eV, figure 1(d).

A very faint dispersionless peak near -3.3 eV for VSe_2, and -2.3 eV for TiS_2 is not $\boldsymbol{k}_\parallel$-dispersive (Starnberg *et al* 1994, 1998). It is probably due to a Frenkel defect state (Pehlke and Schattke 1987b), or three-dimensional DOS.

The remaining peaks are in good qualitative agreement with the calculated structure plots in figure 3. Guided by these plots, we easily rationalized their relation to the valence bands. The experimental intensities differ from PTs in figure 3, or even vanish, mainly due to the variations of $|M_{n'n}|^2$; the difference may also be contributed to by the fact that we have not corrected the reference values of PTs in our VLEED band determination. (For VSe_2, the vanishing intensity from the smaller-PT flat UB near 20 eV in figure 2 may, alternatively, be due to an improper guess of the real line from $-\infty$ to the bottom of this coupling band branch in figure 2(a); it might go along $\mathrm{Re}\, k_\perp = 0$ rather than $|\Gamma\mathrm{A}|$.) The experimental peak broadening is larger than in figure 3, because of the hole-lifetime contribution. This is particularly notable for the lowest-lying Se $4p_z$ and S $3p_z$ bands, where the hole liftime is shortest.

It should be noted that dispersion of the experimental peaks has been very closely reproduced by the calculated structure plots. For TiS_2, we were able to compare our results with the dispersion from previous calculations (Pehlke *et al* 1990a) which used explicit one-

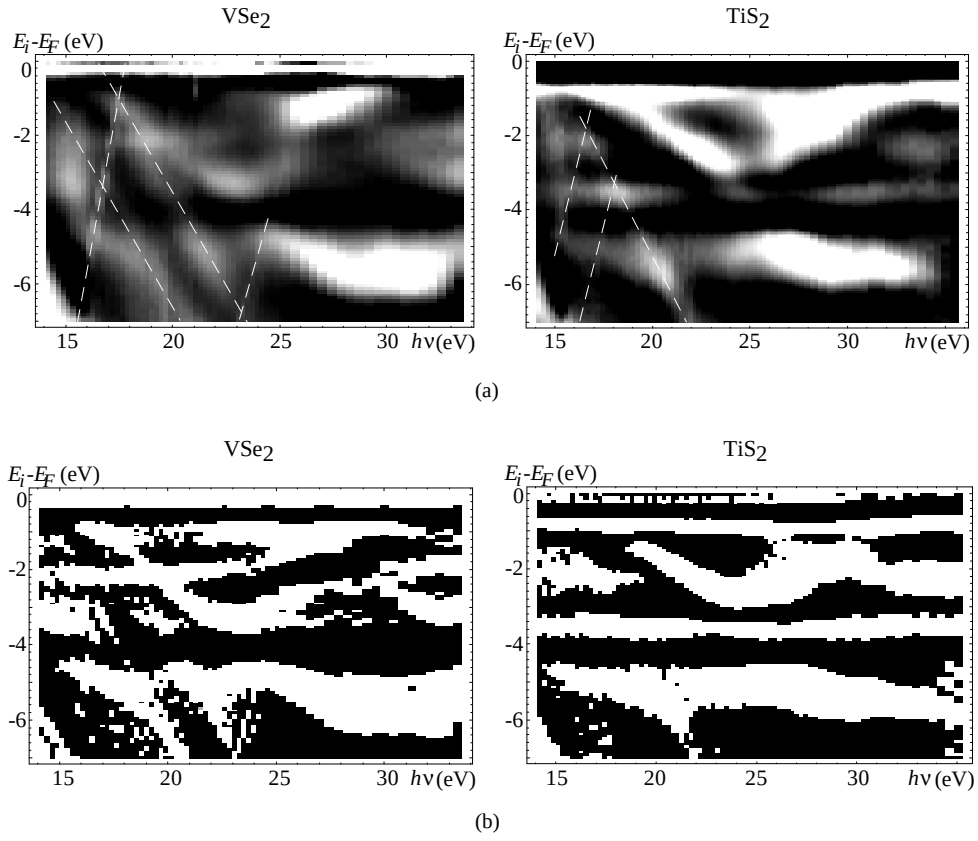

Figure 4. Experimental PE results: (a) PE intensity map, represented in greyscale, with the lighter shade corresponding to the larger intensity. The contrast is increased by subtracting a smooth background, obtained by quadratically weighted averaging within the 2.5 eV wide circles for VSe_2, and 1.5 eV wide for TiS_2. Core level peaks (ascending dashed lines), and SEE peaks (descending dashed lines) are shown. (b) 'Flattened' intensity map: the EDC peaks are shown by white, and the valleys by black irrespective of intensity.

step theory with standard LEED Bloch-wave calculations for the UBs. Although not ideal, our results are radically more relevant; this is by virtue of accurate UBs. We conclude, in contrast to Pehlke *et al* (1990a), that association of the peaks with interband transitions is relevant, although, as we discuss below, at larger $h\nu$ the shifts may be notable.

3.2.2. Shifting of PE peaks from the $k_\perp$-conserving positions. Particularly evident shifts of PE peaks may be seen in our data near valence-band CPs. For example, for TiS_2 the bottom of the S $3p_z^*$ band is reached twice, with $h\nu$ near 24 eV and 34 eV; however, near 34 eV the peak is about 0.3 eV higher in energy, shifted into the band interior. The same is seen for VSe_2. We refer to this effect as the *in-band shifting*.

This effect is in principle included in the one-step theory of PE (Pehlke and Schattke 1989). We here explain its origin from simple physical arguments: A PE peak (1) appears in $\boldsymbol{k}$-space as a Lorentzian $|\Delta_{n'n}|^2$, which is centred in the $k_\perp$-conserving position, and has the $k_\perp$-broadening $2\Delta k_\perp$, $\Delta k_\perp = \mathrm{Im}\, k_\perp^n + \mathrm{Im}\, k_\perp^{n'}$. The $k_\perp$-broadening may be thought of as an intrinsically, not instrumentally, limited resolution in $k_\perp$. Within $2\Delta k_\perp$ the lower-band

dispersion $E(k_\perp)$ is effectively averaged. The origin of the in-band shifting is that near the CPs the averaging makes the PE peak asymmetric, and effectively shifts it into the band interior.

At larger $h\nu$, the final-state component $\mathrm{Im}k_\perp^n$ in the $k_\perp$-broadening increases due to sharply increasing V_i. The in-band shifting increases therefore also. This is clearly seen in our experimental data. We conclude therefore that for TMDCs, generally, the PE bandmapping is accurate only at lower photon energies, $h\nu$ below some 25 eV. Interesting to note, that in a previous work on VSe_2 (Starnberg *et al* 1994, 1998) it was observed that above $h\nu = 40$ eV the broadening of the EDC peaks increases to about the band width, and they became stationary near the band mean energy. This is because due to the increasing $k_\perp$-broadening the in-band shifting becomes extremely large.

Apart from the $k_\perp$-broadening, the observed in-band shifting may also be contributed to by the fact that at higher $h\nu$ the escape length, which is determined by the final-state $1/\mathrm{Im}\,k_\perp^n$, decreases. The PE therefore emerges from the region closer to the surface, where the local DOS at the band edges may be smeared compared to the bulk (Fang *et al* 1997). Attempts to identify this effect are in progress.

Some peaks in our data are shifted from the $k_\perp$-conserving positions despite being far from the CPs. For example, for TiS_2 the S $3p_z$ band below the $h\nu = 25$ eV band looks narrower than this band at higher energies, in-band shifted: the PE intensity is evidently shifted to the top of the band. We attribute this effect to some of the amplitude factors blowing up at the top of the band when combined with large $k_\perp$-broadening (the EDC peaks from this band are broad). Of these factors, the contribution from the $|\mathrm{d}k_\perp^{n'}/\mathrm{d}E|$ variations may not be significant, as it is the same above $h\nu = 25$ eV where the effect is absent. Not significant either is the contribution from the PTs $|T_n|^2$, as the UBs are the same as for the S $3p_z^*$ band below $h\nu = 24$ eV. It is therefore $|M_{n'n}|^2$, which blows up at the top of the band. This behaviour is probably a general effect for the sp bands.

That the variation of $|M_{n'n}|^2$ of the S $3p_z$ band has resulted in such a significant shifting of PE peaks is because of their very large broadening. This is due to large hole absorption $V_i^{n'}$. Having the UB dispersion $E(k_\perp)$ and the absorption V_i^n from VLEED, we could estimate $V_i^{n'}$ from the EDC peak halfwidth $\Gamma_{EDC}/2 = (\mathrm{Im}\,k_\perp^n + \mathrm{Im}k_\perp^{n'})/[(v_{g\perp}^{n'})^{-1} - (v_{g\perp}^{n})^{-1}]$ (Smith *et al* 1993). $v_{g\perp}^{n'}$ was taken as the experimental band width (minimum-to-maximum energy range of the PE peak in the experimental $h\nu$ range) divided by $|\Gamma\mathrm{A}|$. We obtained $V_i^{hole} = 0.30 \pm 0.07$ eV. This figure for the Se $4p_z$ band in VSe_2 is smaller, $V_i^{hole} = 0.06 \pm 0.06$ eV, and the shifting of PE peaks by the amplitude factors is insignificant.

3.2.3. Multiple-band final state composition. For VSe_2, in a wide range 23 eV $< h\nu <$ 31 eV any constant-final-state cut $E_i + h\nu =$ constant in the intensity map shows two dispersive peaks for the same Se $4p_z^*$ band. The peaks merge near 27 eV, enchancing the intensity. These two peaks correspond to the two coupling UBs at the same energy, figure 3, in one final state, which give rise to direct transitions with the two different $k_\perp$. Above $h\nu = 32$ eV one of the peaks vanishes due to $|M_{n'n}|^2$. A similar double-band composition of the final states is observed for TiS_2 in the S $3p_z^*$ band everywhere for $h\nu > 24$ eV; near $h\nu = 27$ eV the peaks merge. The same two UBs are seen in the lowest-lying Se $4p_z$ and S $3p_z$ bands as a very intense and broad structure above $h\nu = 27$ eV. The UBs are not resolved here, because these lower bands are narrower, and give larger hole-lifetime broadening. (Pehlke *et al* (1990a) assigned the double peak D′–D″ at $h\nu = 21.2$ eV to two different UBs. Figure 4(b) shows that D′ is in fact due to SEE.)

3.2.4. PE features near the plasmon threshold. For TiS_2, at the S $3p_z^*$ bottom near $h\nu = 25$ eV the peak dispersion is somewhat irregular, and the intensity varies sharply. The effect may not be due to variations of PTs, because at the S $3p_z$ top near $h\nu = 27$ eV, which correspond to the same UBs, variations are absent. The effect may therefore be due to sharp variations of $|M_{n'n}|^2$. More appealing explanation is however as due to the local field effects (Samuelsen *et al* 1992, Bödicker *et al* 1996). This is supported by the fact that the effect takes place (1) only for upper state energies near the plasmon energy $\hbar\omega_p \approx 21.5$ eV, and (2) only for the S $3p_z^*$ band, which has large dispersion perpendicular to the surface, and is therefore most sensitive to local electromagnetic field variations. Samuelsen *et al* (1992) included the local field effects into the PE calculations within the hydrodynamic model. This has provided better correspondence to the experimental intensities; however, the behaviour near $h\nu = 25$ eV was not reproduced. More elaborate computational modelling is needed to clarify this issue.

3.2.5. Electron–hole interaction. In principle, the excited-state UBs in VLEED may differ from those in PE, because in PE there exists a hole in addition to an excited electron. The energy difference is the electron–hole interaction energy E_{e-h}. To estimate E_{e-h}, we compared the energies of some coupling UBs at Γ and A as seen in VLEED, and in PE. In the PE intensity map, these points are clearly seen as the points of extremal E_i as a function of $h\nu$. The results of this comparison are compiled in table 1. The accuracy of the VLEED energies is limited mainly by our tentative excited-state simulation. The energies may be also shifted by inaccuracy in the workfunction. The accuracy of the PE energies is limited mainly by statistics.

Table 1. Energies of some UBs at Γ and A, obtained by VLEED and PE. PE energies in the same point differ due to the in-band shifting.

VLEED, figure 2(b)	PE, $E_i + h\nu$ from figure 3(a)
VSe_2	
20.1 ± 0.1 (A)	19.8 ± 0.2 (Se $4p_z$ top)
	20.2 ± 0.2 (Se $3p_z^*$ bottom)
28.5 ± 0.3 (Γ)	28.8 ± 0.3 (Se $3p_z^*$ top)
TiS_2	
15.2 ± 0.2 (Γ)	15.4 ± 0.3 (S $3p_z^*$ top)
21.6 ± 0.3 (A)	20.8 ± 0.2 (S $3p_z$ top)
	21.5 ± 0.2 (S $3p_z^*$ bottom)
31.5 ± 0.3 (A)	31.5 ± 0.3 (S $3p_z^*$ bottom; to minimize the in-band shifting, E_i is taken near $h\nu = 24$ eV)

The differences of the VLEED and PE energies were found to be within the experimental inaccuracies. We therefore estimated E_{e-h} for both VSe_2 and TiS_2 to be less than 0.3 eV. Obtaining more accurate figures requires refinement of the excited-state simulation. Small value of E_{e-h} may indicate strong electron and hole delocalization within the layers.

3.3. Bandmapping procedure and the results

For $k_\perp$-resolved bandmapping, as we discussed in 2.4, the PE peaks should be not too broad and well resolved. From the calculated structure plot in figure 3 we have already specified the appropriate, accurate and less-accurate bandmapping, regions. Now, guided by this plot, we found the corresponding regions in the experimental data. For bandmapping we used

the peaks from these regions only, in addition avoiding where the peaks overlap with the peaks from dispersionless bands, or core-level, or SEE peaks. (To be consistent, we did not take into account the hole-lifetime contribution to the peak broadening, which additionally restricts the bandmapping reliability. As we discuss below, this effect particularly severely distorted the bandmapping in the S $3p_{z^*}$ band of TiS_2.)

For VSe_2, the accurate bandmapping peaks in the Se $4p_z$ band are within 16.5 eV $< h\nu <$ 18 eV, and in the Se $4p_z^*$ band within 15 eV $< h\nu <$ 23 eV, excluding narrow overlap with the Se $4p_{x,y}$ band near $h\nu = 19$ eV. The less-accurate, due to larger broadening, peaks in the Se $4p_z$ band are within 22.5 eV $< h\nu <$ 24.5 eV, and in the Se $4p_z^*$ band within 15 eV $< h\nu <$ 23 eV. The less-accurate peaks are also in the Se $4p_z^*$ band with $h\nu >$ 30 eV, where the two UBs are resolved; the accuracy is also limited by rough VLEED band determination in this region. In other regions the peaks are not suitable for bandmapping at all: they are too broad, or overlap with peaks from other valence or UBs, or overlap with core-level or SEE peaks. For TiS_2, the accurate bandmapping peaks in the S $3p_z$ band are within 16 eV $< h\nu <$ 18.5 eV; in the S $3p_z^*$ band within 18 eV $< h\nu <$ 25 eV. The less-accurate peaks in the S $3p_z$ band are within 22 eV $< h\nu <$ 28 eV; in the S $3p_z^*$ band within 25 eV $< h\nu <$ 27 eV. The less-accurate peaks are also in the S $3p_z^*$ band with $h\nu >$ 30 eV, with the two UBs resolved, but the accuracy here is limited by rough VLEED band determination.

To map the lower bands, for the dispersive bands we used all the EDC peaks in the specified regions. For the non-dispersive bands we used the peaks in all regions. For the TiS_2 slightly dispersive bands S $3p_{x,y}$ and S $3p_{x,y}^*$, as the two UBs are not resolved, we used the peaks where only one UB is available. We identified the peak energies numerically as $\mathrm{d}I/\mathrm{d}E = 0$. (We dropped the shoulder-like peaks identified as the minima in $\mathrm{d}^2I/\mathrm{d}E^2$. This required too heavy smoothing of our experimental data, HWHM $\approx$ 0.15 eV, which shifted the peak energies up to $\pm$0.2 eV. A better statistics is needed.) Putting the final-state energies $E_i + h\nu$ of the peaks into the corresponding experimental VLEED UBs in figure 2(b), we obtained their $k_\perp$. (We dropped correcting the VLEED UBs for the electron–hole interaction E_{e-h}, as this figure was within the experimental inaccuracy.)

The results of bandmapping are shown in figure 5 as the experimental points imposed on the LAPW calculated bands. The points from the accurate bandmapping regions are black. The points from the less-accurate regions are grey or, if the corresponding UBs were determined less accurately, crossed. The points, corresponding to the non-dispersive bands, are all black. (We had no experimental points near the bottom of the Se $4p_z$ and S $3p_z$ bands, because there the PE peaks overlap with huge SEE peaks. These points might be resolved in d^2I/dE^2 if the statistics were better.)

3.4. Discussion

3.4.1. Dispersion of the lower bands. For VSe_2, all experimental points from the accurate bandmapping regions show strikingly consistent dispersions in both Se $4p_z$ and Se $4p_z^*$ dispersive bands. The points from the less-accurate regions are somewhat shifted towards the band interiors. This is expected as the larger broadening of these EDC peaks results in notable in-band shifting from the $k_\perp$-conserving positions, as discussed above. This effect is more profound for the Se $4p_z$ band, where the hole-lifetime contribution is larger. The crosses correspond to rough UBs at higher energies. The in-band shifting is clearly seen for them as well.

The experimental points are not, of course, in ideal agreement with the LAPW calculations: the Se $4p_z^*$ band bottom is 0.15 eV below the calculated, and the dispersionless

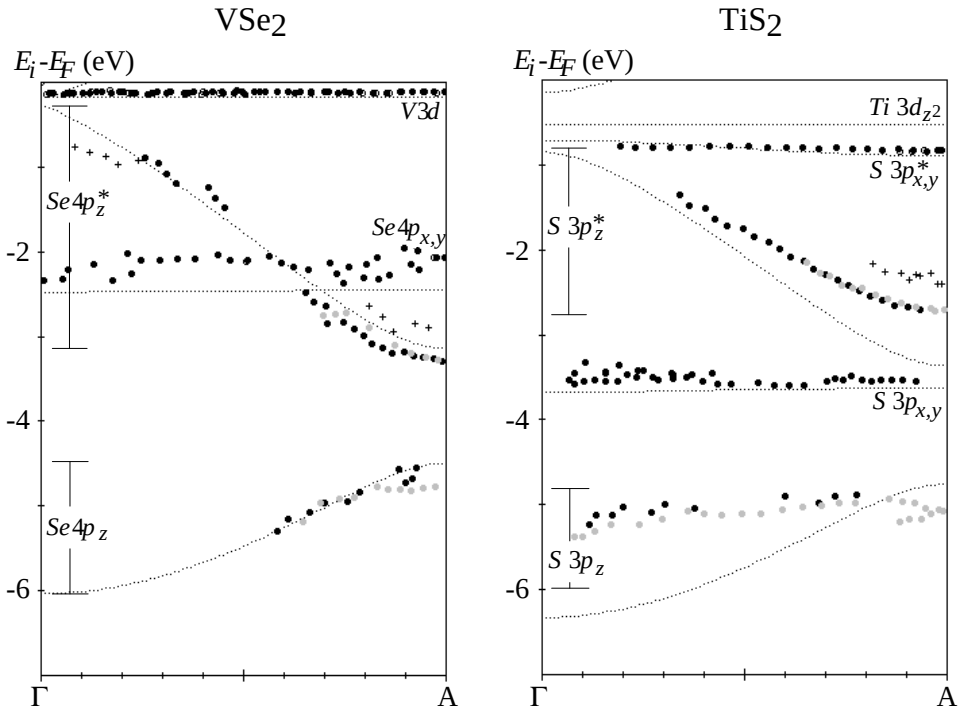

Figure 5. PE bandmapping of the lower bands with the experimental VLEED upper bands, superimposed on the LAPW calculations. The points are from the accurate bandmapping regions (black), and from the less-accurate regions (grey and, where the upper bands were rough, crosses). For TiS_2, the flat experimental dispersion in the S $3p_z$ band shows the shifts of PE peaks caused basically by large hole absorption.

Se $4p_{x,y}$ band is about 0.3 eV above the calculated.

For TiS_2, in the S $3p_z^*$ band the experimental points from both accurate and less-accurate bandmapping regions show very consistent dispersion. The in-band shifting is not seen; it is probably compensated by a minor inaccuracy in the dispersion of the UBs (for TiS_2 the VLEED band determination was less accurate). The points obtained at higher $h\nu$, with roughly determined UBs, are also consistent; they show considerable in-band shifting.

Flatness of the experimental dispersion in the S $3p_z$ band was expected from the analysis in 3.2.2. It is due to large shifts of the PE peaks from the $k_\perp$-conserving positions, which are basically caused by the large hole absorption. (It is not due to any inaccuracy in the UBs, as the same UBs, at least for the points in the less-accurate region, provided consistent mapping of the S $3p_z^*$ band.) In the accurate bandmapping region, the shifts are caused mainly by the $|M_{n'n}|^2$ blowing up closer to the top of the band. In the less-accurate region, the shifts are mainly by the in-band shifting, which is most pronounced near the CPs. To estimate the latter effect, we compared the final-state energies $E_i + h\nu$ at the S $3p_z$ top and at the S $3p_z^*$ bottom, table 1, which correspond the same point in UBs. The difference is 0.7 eV, of which more than half is the in-band shifting at the S $3p_z$ top; this effect is seen to displace the experimental S $3p_z$ top by 0.15|ΓA| from A.

Comparing to the LAPW calculations, the bottom of the S $3p_z^*$ band is experimentally 0.6 eV above the calculated. Also the bottom of the S $3p_z$ band, estimated near $h\nu = 35$ eV

as −5.6 eV and roughly corrected from the in-band shifting, is about 0.5 eV above the calculated. The Ti $3\,d_{z^2}^2$ band is not mapped in figure 5, as it produced only a slight shoulder-like peak not resolved in dI/dE. In figure 4(b) this band is seen as slightly dispersive, and placed 0.1 eV below E_F, which is 0.4 eV above the calculated.

Overall, the consistency of our experimental $E(k_\perp)$, in particular for VSe_2, is in strong contrast to the previous results obtained with free-electron-like UBs, which, despite empirical adjustments, produced strongly scattered points in the valence band. Evidently, the crucial point has been accurate experimental determination of the UBs by VLEED. We stress, that our results are free from any adjustable parameters, as the UBs were determined in an independent VLEED experiment.

3.4.2. Irrelevance of free-electron-like and ground-state UBs. Empirical free-electron-like UBs are not, in general, appropriate for TMDCs. As we discussed above, these materials are characterized by multiple-branch coupling UBs, and the free-electron fit of each branch strongly depends on E and $\boldsymbol{k}_\parallel$. To illustrate, for VSe_2 even the best free-electron fit along ΓA in our $h\nu$ range would give the $k_\perp$-error up to $0.6|\Gamma A|$ (maximal in the flat UB at $E_i + h\nu \approx 13$ eV). This error is incompatible with any accurate bandmapping. For TiS_2 the error is even larger. The free-electron approximation is not therefore able to allow for any consistent bandmapping.

Ground-state-calculated UBs, even if excited-state smoothing is simulated, are also inappropriate without the experimental VLEED corrections. Apart from correcting the computational inaccuracies, the experimental data introduces significant self-energy corrections of 0.5–1 eV. To illustrate, our calculated LAPW UBs would give the $k_\perp$-error up to $0.5|\Gamma A|$ (again maximal in the flat UB at $E_i + h\nu \approx 13$ eV). For TiS_2 the error would again be larger, because of less accurate calculations.

3.4.3. Extending the VLEED-PE absolute bandmapping: layer-parallel dispersion $E(\boldsymbol{k}_\parallel)$. So far the $E(\boldsymbol{k}_\parallel)$ mapping on TMDCs has been performed in the EDC mode, varying $\boldsymbol{k}_\parallel$; $k_\perp$ was indeterminate. Our scheme of the VLEED-PE absolute bandmapping circumvents this problem, allowing for determination of $k_\perp$ for any $\boldsymbol{k}_\parallel$ from the corresponding off-normal VLEED spectra.

Of particular interest would be accurate mapping of $E(\boldsymbol{k}_\parallel)$ keeping $k_\perp$ in the BZ symmetry planes, KM or AHL. Here we suggest a straight experiment, which extends the band gap emission PE technique (Courths *et al* 1989). First, one performs the VLEED measurements varying $\boldsymbol{k}_\parallel$ to find the intersections of the coupling UBs with the symmetry planes as functions of $\boldsymbol{k}_\parallel$, $E^{sym}(\boldsymbol{k}_\parallel)$. Second, one performs PE measurements varying $\boldsymbol{k}_\parallel$, using the CFS mode with the final-state energies following $E^{sym}(\boldsymbol{k}_\parallel)$. $E(\boldsymbol{k}_\parallel)$ is being measured then exactly in the symmetry planes.

4. Conclusion

The layer-perpendicular dispersions $E(k_\perp)$ of the typical layered TMDCs VSe_2 and TiS_2 were studied by an absolute band structure determination method, combining VLEED determination of the upper bands (UBs) with PE bandmapping of the lower bands.

VLEED determination of the UBs employed: (1) a simple reference calculation of $E(k_\perp)$ and the dT/dE spectrum, based on ground-state LAPW calculations; (2) from comparing the reference dT/dE with the experimental dT/dE, adjusting the reference $E(k_\perp)$; (3) simulation of the excited-state effects. The procedure may be improved

if based on excited-state reference calculations, at least empirical. We found that the coupling (mainly contributing in VLEED and PE) UBs are characterized by large self-energy corrections, feature two main branches and are compatible neither with free-electron approximation, nor with ground-state calculations.

Knowledge of the UBs allowed us to specify the optimal, rather restrictive, regimes for $k_\perp$-resolved PE bandmapping. The corresponding experimental PE data were represented as a map of the PE intensity as a function of E_i and $h\nu$, which helped consistent rationalization of the valence-band peaks. We found that the general behaviour of the PE intensity is well described by direct, $k_\perp$-conserving, transitions to the coupling UBs. In particular, we identified double-peak PE structures from the final states composed of two UBs. Finer details of the PE intensity are basically the consequences of an excited-state effect, the peak broadening due to finite electron and hole lifetime. In particular, we identified the in-band shifting of PE peaks, which is due to effective averaging of $E(k_\perp)$ within the $k_\perp$-broadening. To minimize the influence of this effect in PE bandmapping, for TMDCs it should employ photon energies below 25 eV. Another interesting effect is the distorted dispersion in the TiS_2 S $3p_z$ band, which is certainly due to the sharp matrix element variation within the peak width.

Finally, we performed explicit mapping of the valence band $E(k_\perp)$ using the well resolved PE peaks in the regions of small $k_\perp$-broadening, and the experimental VLEED UBs. The obtained $E(k_\perp)$, except for the distorted TiS_2 S $3p_z$ band, is very consistent and in overall agreement with the LAPW calculations, in contrast to previous attempts at bandmapping from empirical free-electron-like UBs. The crucial point to achieve accurate bandmapping has been the independent VLEED determination of the very complicated UBs.

References

Anderson O, Manzke R and Skibowski M 1985 *Phys. Rev. Lett.* **55** 2188
Bödicker A, Leventi-Peetz A and Schattke W 1996 *J. Electron. Spectrosc.* **78** 481
Capart G 1969 *Surf. Sci.* **13** 361
Claessen R, Ellis W P, Janowitz C, Olson C G, Shen Z X, Eyert V, Skibowski M, Friemelt K, Bucher E and Schattke W 1996 *Phys. Rev.* B **54** 2453
Courths R, Wern H, Leschik G and Hüfner S 1989 *Z. Phys.* B **74** 233
Fang C M, de Groot R A and Haas C 1997 *Phys. Rev.* B **56** 4455
Feibelman P J and Eastman D E 1974 *Phys. Rev.* B **10** 4932
Friend R F and Yoffe A D 1987 *Adv. Phys.* **36** 1
Goldmann A, Altmann W and Dose V 1991 *Solid State Commun.* **79** 511
Jaklevic R C and Davis L C 1982 *Phys. Rev.* B **26** 5391
Jepsen D W, Himpsel F J and Eastman D E 1982 *Phys. Rev.* B **26** 4039
Krasovskii E E and Schattke W 1997 *Phys. Rev.* B **56** 12 874
Langlais V, Belkhir H, Themlin J-M, Debever J-M, Yu L M and Thiry P A 1995 *Phys. Rev.* B **52** 12 095
Law A R, Andrews P T and Hughes H P 1991 *J. Phys. C: Solid State Phys.* **3** 813
Matzdorf R 1996 *Appl. Phys.* A **63** 549
Pehlke E, Samuelsen D and Schattke W 1990a *Vacuum* **41** 55
Pehlke E and Schattke W 1987a *J. Phys. C: Solid State Phys.* **20** 4437
——1987b *Z. Phys.* B **66** 31
——1989 *Solid State Commun.* **69** 419
Pehlke E, Schattke W, Anderson O, Manzke R and Skibowski M 1990b *Phys. Rev.* B **41** 2982
Pendry J B 1974 *Low Energy Electron Diffraction* (London: Academic)
——1976 *Surf. Sci.* **57** 679
Samuelsen D, Pehlke E, Schattke W, Andersen O, Manzke R and Skibowski M 1992 *Phys. Rev. Lett.* **68** 522
Smith N V, Thiry P and Petroff Y 1993 *Phys. Rev.* B **47** 15 476
Starnberg H I, Brauer H E, Holleboom L J and Hughes H P 1993 *Phys. Rev. Lett.* **70** 3111
Starnberg H I, Brauer H E, Holleboom L J, Strocov V N and Hughes H P 1998 *Phys. Rev.* B submitted

Starnberg H I, Brauer H E, Nilsson P O, Holleboom L J and Hughes H P 1994 *Mod. Phys. Lett.* **8** 1261
Straub D, Skibowski M, Himpsel F J and Drube W 1985 *Phys. Rev.* B **31** 8254
Strocov V N 1991 *Solid State Commun.* **78** 545
——1995 *Int. J. Mod. Phys.* B **9** 1755
——1996 *Meas. Sci. Technol.* **7** 1636
——1998 *Solid State Commun.* **106** 101
Strocov V N and Starnberg H 1995 *Phys. Rev.* B **52** 8759
Strocov V N, Starnberg H I and Ettema A R F 1995 *Solid State Commun.* **96** 659
Strocov V N, Starnberg H and Nilsson P O 1996a *J. Phys.: Condens. Matter* **8** 7539
——1996b *J. Phys.: Condens. Matter* **8** 7549
Strocov V N, Starnberg H and Nilsson P O 1997a *Phys. Rev.* B **56** 1717
Strocov V N, Starnberg H, Nilsson P O, Brauer H E and Holleboom L J 1997b *Phys. Rev. Lett.* **79** 467